Journal of Low Temperature Physics
https://doi.org/10.1007/s10909-020-02418-1

The Superconductivity Mechanism in Nd-1111 Iron-Based Superconductor Doped by Calcium

F. Shahbaz Tehrani[1] · V. Daadmehr[1]

Received: 9 August 2019 / Accepted: 16 February 2020
© Springer Science+Business Media, LLC, part of Springer Nature 2020

Abstract
We describe the effect of nonmagnetic impurity on the superconductivity behavior of the $NdFeAsO_{0.8}F_{0.2}$ iron-based superconductor. The resistivity measurements show that the superconductivity is suppressed upon increasing the low amounts of calcium impurity ($x \leq 0.05$). Also, the T_C decreases with the increase in the residual resistivity. Such behavior is qualitatively described by the Abrikosov–Gorkov theory and confirms that these impurities act as scattering centers. Moreover, we present the phase diagram of our synthesized samples for the various calcium dopings. We find that according to the increase in the calcium impurities and the decrease in the spin-density wave transition tempeθrature (T_{SDW}), Fe ions are arranged stripe-antiferromagnetic at lower temperatures and also the superconducting transition temperature (T_C) declines. Based on our results and in agreement with the available theories as is explained in the text, since the S_{++} state has no effect on the impurity-doped samples, and for low amounts of calcium, the $S_{\pm}$ state that is attributed to the spin-fluctuations causes the superconductivity suppression. So, it confirms the role of the spin-fluctuations as a dominant pairing mechanism in our synthesized samples.

Keywords Superconductivity · Iron-based superconductor · Pairing mechanism · Spin-fluctuations

✉ V. Daadmehr
daadmehr@alzahra.ac.ir

F. Shahbaz Tehrani
tehrani66@gmail.com
http://staff.alzahra.ac.ir/daadmehr/

[1] Magnet and Superconducting Research Lab, Faculty of Physics and Chemistry, Alzahra University, Tehran 19938, Iran

Published online: 25 March 2020

1 Introduction

For the first time, the discovery of superconductivity in $LaFeAsO_{1-x}F_x$ compounds (with $T_C = 26$ K) by Y. Kamihara et al. [1] attracted the attention of physicists to the iron-based superconductors (FeSCs) as a new group of superconductors and introduced them as a candidate for another group of high-temperature superconductors. The FeSCs have similar characteristics to the cuprates such as the layered structure, the small coherence length, the dependence of the superconductivity transition temperature (T_C) upon doping and the unconventional pairing mechanism [2–6]. Also, they display the extraordinary physics due to the co-existence of magnetism and superconductivity, and the multiband electronic structure [7, 8]. But the superconducting mechanism of these compounds is one of the controversial issues, and there is still no explicit answer to this question. Most FeSCs have a common phase diagram that there is often a structural transition from tetragonal to orthorhombic and a magnetic spin-density wave (SDW) state that the spin configuration is striped antiferromagnetic (AFM) [9–12]. From this, one can conclude that they play an important role in the superconducting mechanism of FeSCs. However, the cause of the structural transition is still under debate and has been proposed that either spin [13–15] or ferro-orbital nematic ordering [16–18] is responsible for the occurrence of it. In the spin-nematic scenario, the structural transition is driven by magnetic fluctuations and the lattice symmetry breaks from C_4 to C_2 through the magnetic-elastic coupling to lift the degeneracy of the stripe-type antiferromagnetism [19–22]. In the orbital-nematic scenario, the ferro-orbital ordering causes the breaking of C_4 symmetry and the strong inter-orbital interactions lead to an unequal occupation of the d_{xy} and d_{yz} Fe orbitals [23–25].

Moreover, up to now, two superconducting mechanisms have been reported for the FeSCs: spin- and orbital-fluctuations. Based on the spin-fluctuations theory, fully gapped sign-reversing s-wave ($S_{\pm}$) state had been predicted [26, 27]. The origin of the spin-fluctuations is the intra-orbital nesting and the Coulomb interaction. Furthermore, the orbital-fluctuations generally originate from the inter-orbital nesting and the electron–phonon interactions due to the Fe–ion optical phonons [28–30]. The theories introduced that the electron–phonon coupling improves the orbital-fluctuations at wave vectors (0, 0) and (π, 0)/(0, π), which correspond to ferro-orbital and antiferro-orbital-fluctuations, respectively [31, 32]. Also, the antiferro-orbital-fluctuations around (π, 0)/(0, π) compete with the antiferromagnetic spin-fluctuations around the same wave vectors [5]. When the spin-fluctuations dominate, the pairing state is $S_{\pm}$ as mentioned above, but when the orbital-fluctuations dominate, the sign of the gap remains the same between the electron and hole pockets and is called the S_{++} state [33–35].

The theoretical models [33, 36–38] described that the $S_{\pm}$ state is very fragile to the nonmagnetic impurities, and only 1% nonmagnetic impurity with moderate scattering potential could completely suppress superconductivity and the $S_{\pm}$ pairing state, while for the S_{++} symmetry the T_C does not show the effective variation to the nonmagnetic impurities [33]. So, an appropriate probe to determine the type

of symmetry and pairing in the FeSCs is the substitution of nonmagnetic impurity. Consequently, to discover the superconducting mechanism, several experimental works have been carried out for the investigation of the impurity effects on the suppression of superconductivity in the FeSCs [10, 39–43]. For example, the Zn ions act as strong potential scattering centers in the $LaFeAsO_{1-x}F_x$ compound and suppress the superconductivity [44]. However, the conclusions remain discussible and more experimental and theoretical works are needed to illuminate the impurity effects in the FeSCs that can help us to understand the superconducting mechanism. In our previous work, we studied the effects of Ca^{2+}/Nd^{3+} substitution on polycrystalline $Nd_{1-x}Ca_xFeAsO_{0.8}F_{0.2}$ samples with $0 \leq x \leq 0.1$ [45]. We compared our experimental data and the results of the mentioned theories, i.e., the spin- and orbital-fluctuations in the pairing mechanism. The consistency of our experimental results and the theoretical reports based on the spin- and the orbital-fluctuations theories has shown that these models play an important role in the pairing mechanism of the iron-based superconductors. Given this background, in this work, we focus on the investigation of calcium doping effects as a nonmagnetic impurity in the superconductivity mechanism of Nd-1111 iron-based superconductor. We study the calcium doping effects on the structural transition and SDW state and the relation between them to clarify the superconducting mechanism. We show that the calcium doping can affect the spin- and orbital-fluctuations and change the competition between them. We hope that the comparison of our experimental results and the available corresponding theories will help to understand the pairing symmetry and superconductivity mechanism in the FeSCs.

2 Experimental

We used one-step solid-state reaction method for synthesizing the polycrystalline samples with the nominal compositions of $Nd_{1-x}Ca_xFeAsO_{0.8}F_{0.2}$ ($x = 0.0$, 0.01, 0.025, 0.05) as described in our previous works in Refs. [46, 47]. The $NdFeAsO_{0.8}F_{0.2}$, $Nd_{0.99}Ca_{0.01}FeAsO_{0.8}F_{0.2}$, $Nd_{0.975}Ca_{0.025}FeAsO_{0.8}F_{0.2-}$ and $Nd_{0.95}Ca_{0.05}FeAsO_{0.8}F_{0.2}$ samples are labeled as Nd-1111, Nd–Ca0.01, Nd–Ca0.025 and Nd–Ca0.05, respectively. The neodymium powder (99.99%), arsenic pieces (99.99%), Fe_2O_3 (99.9%), FeF_3 (99%), Fe (99.99%) and CaF_2 (99%) powders were utilized as precursor materials. The stoichiometric amounts of these materials were mixed and grounded for 2 h. The homogenous mixtures were pressed into pellets with 10 mm diameter and were sealed in evacuated quartz tubes. All the processes were performed in a glove box with nitrogen atmosphere. The heating process of the sealed tubes was carried out with a slow heating rate in four steps: 350 °C/5 h, 640 °C/14 h, 880 °C/20 h and 1150 °C/20 h. After that, the synthesized samples were again grounded, re-pelletized and sealed in evacuated quartz tubes. Finally, the heating process was repeated.

The X-ray diffraction patterns (XRD) of our samples were accomplished using a PANalytical® PW3050/60 X-ray diffractometer with Cu Kα radiation ($\lambda = 1.54056$ Å) operated at 40 kV and 40 mA with a step size of 0.026°. The refinement method

of Rietveld was applied with the "Material Analysis Using Diffraction" (MAUD) program (v.2.8). We applied a four-probe technique for the superconductivity measurements using the 20 K Closed Cycle Cryostat (QCS101), ZSP Cryogenics Technology. Also, we used a Lake Shore-325 temperature controller for measuring the temperature and the applied DC current (Lake Shore-120) was 10 mA, and the voltage was measured with microvolt accuracy. The important temperatures for preparation of our samples were chosen based on the TG-DTG and DTA measurements that are shown in Ref. [46]. The result of this choosing is an increase in the crystalline quality of our samples, as illustrated in the XRD patterns and confirmed according to the Rietveld's analysis (see Fig. 4 in Ref. [45]). As shown in the XRD pattern, the dominant impurity phase does not exist and predicates the high quality for the Nd-1111 sample (see Fig. 1).

3 Results and discussion

Figure 1 shows the XRD patterns of the $Nd_{1-x}Ca_xFeAsO_{0.8}F_{0.2}$ samples. All samples have the tetragonal structure with P4/nmm:2 space group that was proved with Rietveld's analysis by employing the MAUD software. Based on the MAUD analysis, the Ca^{2+} ions are substituted completely in the Nd^{3+} sites (see Table 1). Also, there are some undesirable phases in our samples that the volume percent (Vol.%) of them is calculated (4.5–11.7 Vol.%) and then listed in Table 2. It shows that the impurities slightly exist in our samples. Figures 2 and 3a–c display the XRD patterns of the Nd-1111 and the doped samples that are refined by the MAUD analysis and approve the formation of the FeSC desired phase in each sample. The S parameter proves the goodness of the refinement quality that is defined by $S = R_{wp}/R_{exp}$, where R_{wp} is the weighted residual error and R_{exp} is the expected error. Whatever the S is closer to

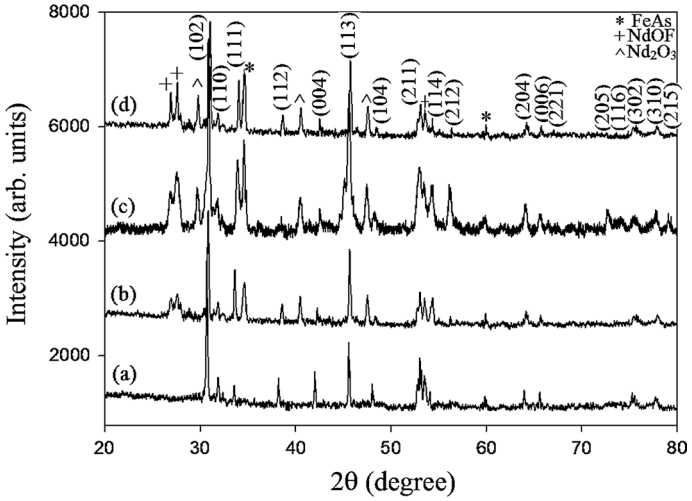

Fig. 1 The XRD patterns of our samples: **a** Nd-1111, **b** Nd–Ca0.01, **c** Nd–Ca0.025 and **d** Nd–Ca0.05

Table 1 The ideal structural parameters and the experimental-refined values from MAUD software for the $Nd_{1-x}Ca_xFeAsO_{0.8}F_{0.2}$ samples

Sample name	The ideal structural parameters					The experimental-refined values				
	Ions	Position			Occupancy	Ions	Position			Occupancy
		x	*y*	*z*			*x*	*y*	*z*	
Nd-1111	Nd^{3+}	0.25	0.25	0.1385	1	Nd^{3+}	0.2499	0.2499	0.1381	0.9998
	Fe^{2+}	0.75	0.25	0.5	1	Fe^{2+}	0.75	0.25	0.5	1
	As	0.25	0.25	0.6574	1	As	0.25	0.25	0.6574	1
	O^{2-}	0.75	0.25	0	0.8	O^{2-}	0.75	0.25	0	0.8
	F^{-}	0.75	0.25	0	0.2	F^{-}	0.75	0.25	0	0.2
Nd–Ca0.01	Ca^{2+}	0.25	0.25	0.1385	0.01	Ca^{2+}	0.2498	0.2499	0.1379	0.0105
	Nd^{3+}	0.25	0.25	0.1385	0.99	Nd^{3+}	0.2497	0.2499	0.1374	0.9866
	Fe^{2+}	0.75	0.25	0.5	1	Fe^{2+}	0.75	0.25	0.5	1
	As	0.25	0.25	0.6574	1	As	0.25	0.25	0.6574	1
	O^{2-}	0.75	0.25	0	0.8	O^{2-}	0.75	0.25	0	0.8
	F^{-}	0.75	0.25	0	0.2	F^{-}	0.75	0.25	0	0.2
Nd–Ca0.025	Ca^{2+}	0.25	0.25	0.1385	0.025	Ca^{2+}	0.2498	0.2498	0.1377	0.0239
	Nd^{3+}	0.25	0.25	0.1385	0.975	Nd^{3+}	0.2497	0.2496	0.1372	0.9746
	Fe^{2+}	0.75	0.25	0.5	1	Fe^{2+}	0.75	0.25	0.5	1
	As	0.25	0.25	0.6574	1	As	0.25	0.25	0.6574	1
	O^{2-}	0.75	0.25	0	0.8	O^{2-}	0.75	0.25	0	0.8
	F^{-}	0.75	0.25	0	0.2	F^{-}	0.75	0.25	0	0.2
Nd–Ca0.05	Ca^{2+}	0.25	0.25	0.1385	0.05	Ca^{2+}	0.2497	0.2499	0.1376	0.0489
	Nd^{3+}	0.25	0.25	0.1385	0.95	Nd^{3+}	0.2496	0.2496	0.1370	0.9506
	Fe^{2+}	0.75	0.25	0.5	1	Fe^{2+}	0.75	0.25	0.5	1
	As	0.25	0.25	0.6574	1	As	0.25	0.25	0.6574	1
	O^{2-}	0.75	0.25	0	0.8	O^{2-}	0.75	0.25	0	0.8
	F^{-}	0.75	0.25	0	0.2	F^{-}	0.75	0.25	0	0.2

Table 2 The parameters that are obtained from the MAUD analysis

Sample	Vol.%. of phases				R_{wp} (%)	R_{exp}(%)	S
	Pure	FeAs	NdOF	Nd_2O_3			
Nd-1111	81.5	10.7	7.8	0	5.713	3.323	1.719
Nd–Ca0.01	77.0	9.8	8.7	4.5	6.001	3.214	1.867
Nd–Ca0.025	74.2	11.4	8.5	5.9	7.715	3.531	2.185
Nd–Ca0.05	73.8	11.7	7.7	6.7	4.656	3.411	1.365

1, confirms the goodness of refinement. These parameters are displayed in Table 2, and it can be found that the obtained results from the MAUD analysis are valid. The variation of lattice parameters "*a*, *c*" and the cell volume (that are obtained from the MAUD calculations) for the calcium contents is displayed in Fig. 4. All the data are

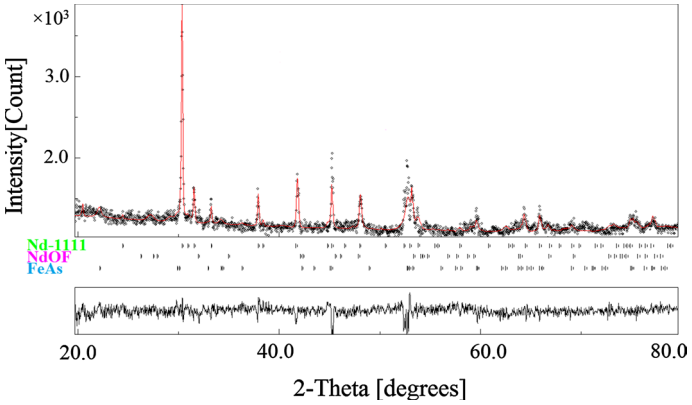

Fig. 2 The XRD pattern of Nd-1111 sample that is refined using the MAUD software

normalized by the values of the undoped sample, i.e., Nd-1111. It is seen that the lattice parameters and the cell volume decrease upon increasing the calcium doping. The decline of the lattice parameter "*c*" is more in comparison with the "*a*." Due to the small difference in the ionic radius of the calcium and neodymium ions, the reason for the reduction in the mentioned parameters is the change in other structural parameters such as bond lengths, bond angles and the thickness of the layers. In our previous work, we explicitly explained the reason for the reduction in the lattice parameters, based on the variation of bond lengths, bond angles and the thickness of layers with the increase in the calcium content [45]. The temperature dependence of resistivity for our synthesized samples is shown in Fig. 5a–d. As shown in these figures, the T_C of our samples decreases by increasing the calcium doping and also, the superconductivity suppresses in the Nd–Ca0.05 sample. In our previous work [45], the dependence of T_C and the As–Fe–As bond angles, the Fe–As bond length, the pnictogen height and the lattice parameters for the various calcium contents have been discussed. We have understood that the T_C decreased with increase in the distortion of FeAs4-tetrahedron from the regular value and also with decrease in the Fe-As bond length, the pnictogen height, and the lattice parameters with the increase in the calcium contents. Our experimental data were consistent with the same results that had suggested theoretically based on the spin- and orbital-fluctuations theories (as described in Ref. [45]). Now, we want to know which type of the spin- or orbital-fluctuations is dominating in our samples, so we study the investigation of calcium impurity effects via the available theories.

Suppression of superconductivity by nonmagnetic impurity—From the XRD data, we can see that the calcium content could be easily placed into the neodymium sites of Nd-1111 sample up to 0.05 [45]. According to Abrikosov–Gorkov theory (AG), if the impurities act as strong pair breakers, the suppression of T_C is associated with the impurity scattering rate defined as $k_B \Delta T_C \approx \pi\hbar/\tau_s \propto \rho_0$, where k_B is Boltzmann constant, ΔT_C is the variation of the T_C in comparison with the sample without impurity, $\hbar = h/2\pi$ that h is Planck's constant, τ_s is the time of electron travel without spin-flip, and ρ_0 is the residual resistivity. The ρ_0 value obtains from

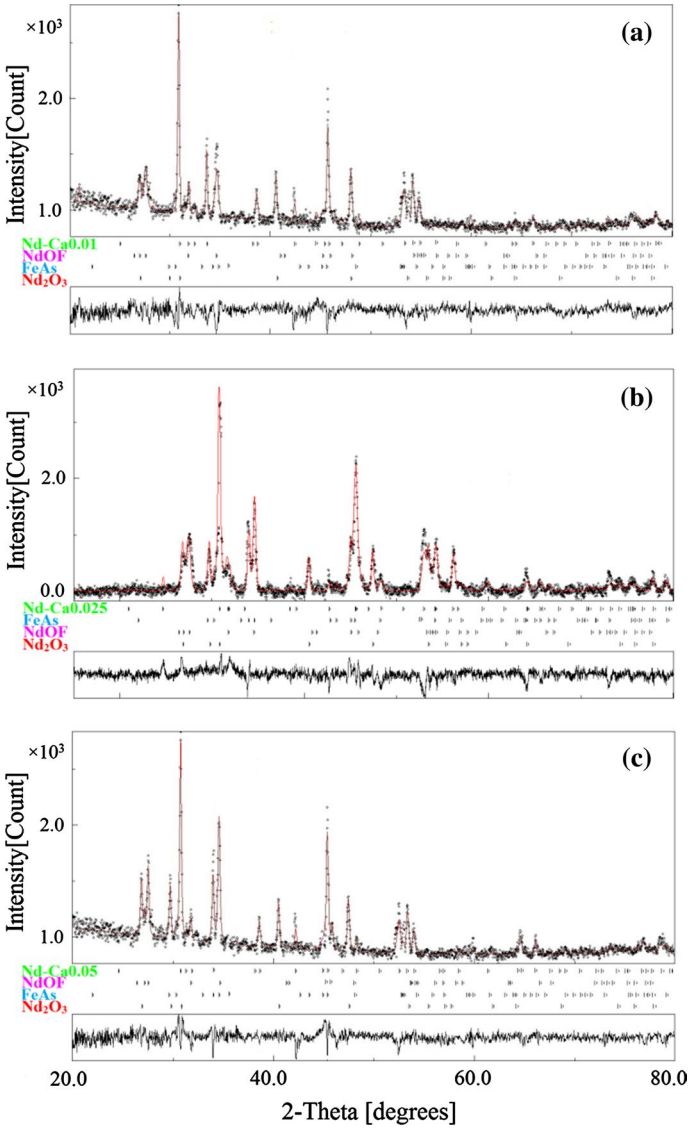

Fig. 3 The XRD patterns that are refined using the MAUD software for **a** Nd–Ca0.01, **b** Nd–Ca0.025 and **c** Nd–Ca0.05 doped samples

the extrapolation of $\rho(T)$ curve before starting of the superconductivity state [40] that is displayed for our synthesized samples by a dashed line in Fig. 5a–d. Figure 6 displays that the values of ρ_0 and the normalized T_C are found to increase and decrease, respectively, by increasing the calcium impurity. Also, the decrement of the normalized T_C versus the calcium doping is linear with a good approximation. Furthermore, the dependence of T_C and ρ_0 is shown in Fig. 7, which describes the

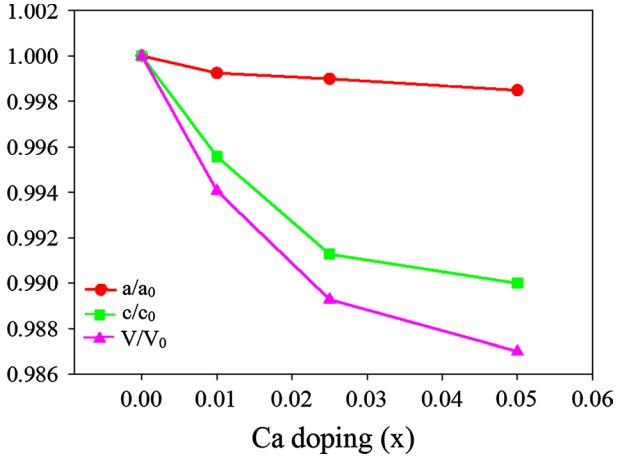

Fig. 4 The variation of normalized lattice parameters and cell volume for the various calcium doping

suppression of superconductivity in our synthesized samples with the increment of ρ_0. So, the substitution of calcium ions strongly destroys the superconductivity and increases the residual resistivity (ρ_0) for our samples, which means that these impurities act as scattering centers.

Based on the AG theory, in the presence of nonmagnetic impurities and isotropic exchange interaction, the variation of T_C is given by the following expression [48–51]:

$$\ln\left[\frac{T_C}{T_{C0}}\right] = \Psi\left[\frac{1}{2} + (2\pi k_B T_C \tau_s)^{-1}\right] - \Psi\left(\frac{1}{2}\right) \tag{1}$$

with

$$\frac{1}{\tau_s} = 2\pi n_I N(0)(g-1)^2 J_{exc}^2 J(J+1) \tag{2}$$

where n_I is the concentration of impurity ions, T_{C0} is the transition temperature in the absence of doping, Ψ is the digamma function, $N(0)$ is the density of states at the Fermi level, and τ_s is the time of electron travel without spin-flip. Also, g and J are the Lande g factor and the total angular momentum of the impurity ion, respectively. Likewise, J_{exc} is the exchange constant between the impurity ion spin and the conduction electron spin. For the small concentration of nonmagnetic impurities, the T_C decreases linearly with n_I and the initial rate of depression of T_C (dT_C/dn_I) is determined by the following equation [48, 51]:

$$\frac{dT_C}{dn_I}\Big|_{n_{I\to 0}} = \frac{dT_c}{dx}\Big|_{x\to 0} = -\frac{\pi^2 N(0) J_{exc}^2 (g-1)^2 J(J+1)}{2k_B} \tag{3}$$

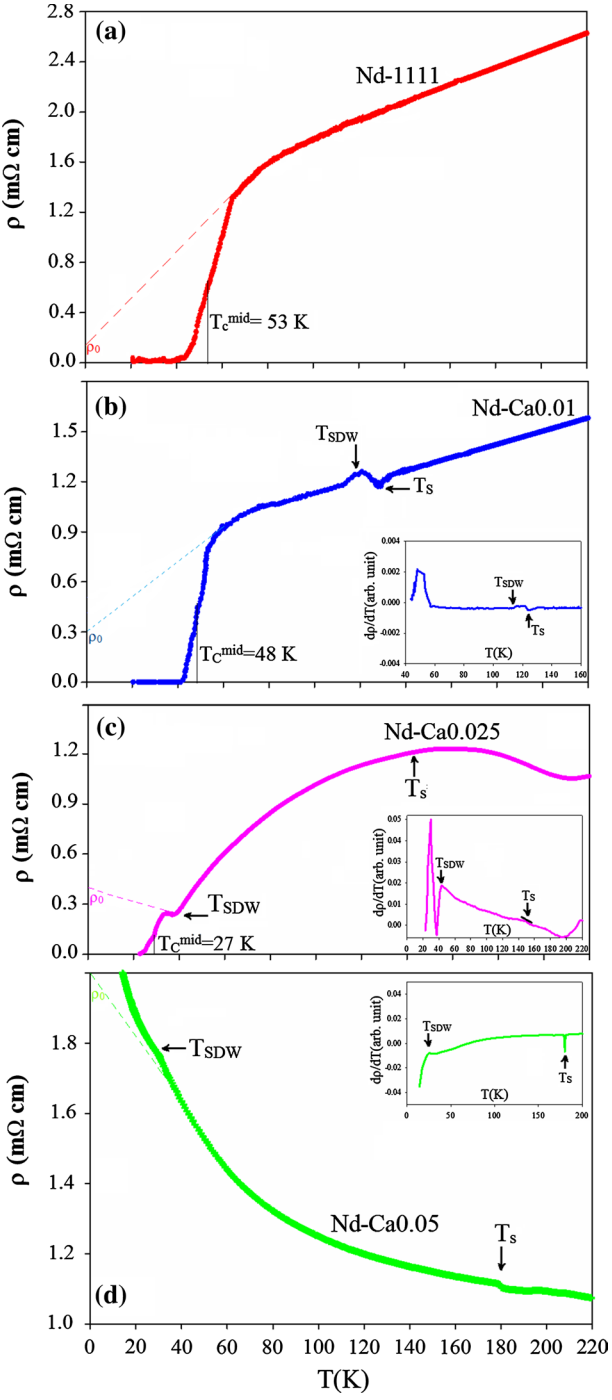

Fig. 5 Temperature dependence of resistivity for **a** the Nd-1111, **b** Nd–Ca0.01, **c** Nd–Ca0.025 and **d** Nd–Ca0.05 samples (the dash line determines the ρ_0 that is the residual resistivity. See text for more details). Also, the insets show the variation of dρ/dT for each sample

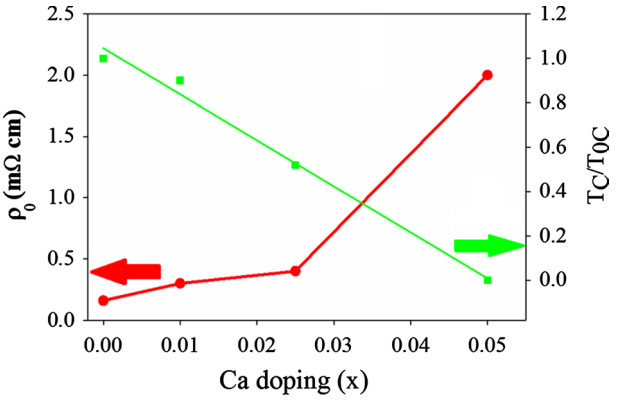

Fig. 6 The variation of ρ_0 and T_C/T_{C0} as a function of calcium contents (x)

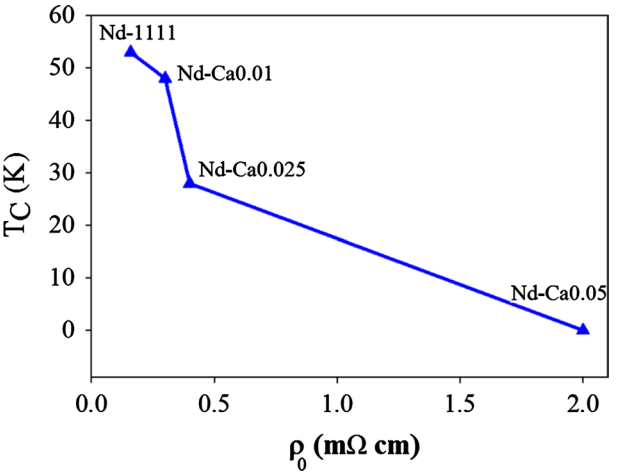

Fig. 7 The dependence T_C of versus ρ_0 for our synthesized samples

For $Nd_{1-x}Ca_xFeAsO_{0.8}F_{0.2}$ samples with one dopant atom per unit cell, we define $x = n_I$ where x is the fraction of calcium ions in our synthesized samples. The variation of T_C with the concentration of calcium doping is shown in Fig. 6. With the calculation of line slope (by using the experimental value), we have $\frac{dT_c}{dx}$ = -81.15 K/atom and so obtain from Eq. (3):

$$N(0)J_{exc}^2 \approx 70.9 \times 10^{-5} \left(\frac{eV \cdot \text{states}}{\text{atom spin}} \right) \tag{4}$$

We get a value of $N(0) = 10$ ($\frac{\text{states}}{eV \cdot \text{atom spin}}$) from Ref. [52]. Therefore, the exchange constant (J_{exc}) between the calcium ion spin and the conduction electron spin is estimated as |8| meV. This amount has the same order of magnitude for the 122-type of

FeSCs and the conventional superconductors in Refs. [53, 54] that is obtained based on the ESR experiments [43]. The dependence result of T_C (ρ_0) and based on the AG theory shows that calcium impurity ions behave similar to the magnetic ions with J_{exc} = |8| meV in our samples. Consequently, the AG theory describes the competition effects of the magnetic and nonmagnetic impurities in the superconductivity destruction.

Phase diagram of the synthesized samples—As shown in Fig. 5b–d, there are other shoulders in the resistivity measurements of the calcium-doped samples. These shoulders were usually attributed to the structural transition (T_S) and the SDW state (T_{SDW}) [55]. In 1111-type of FeSCs, the T_{SDW} is smaller than T_S [56], while for the 122-type is the same and they move away from each other by substitution of the doping and applying pressure [57]. For higher accuracy, we calculate the derivative of resistivity and obtain the values of T_S and T_{SDW} for our synthesized samples (see the inset of Fig. 5b–d and Table 3). The phase diagram of our samples is displayed in Fig. 8a and shows the suppression of the superconducting transition and the SDW state with increase in the calcium impurities, while the T_S increases. The structural and magnetic phase transitions have been measured by neutron diffraction on the polycrystalline samples of the 1111-type [55, 58]. The peaks in these data can be described based on the magnetic unit cell with the chains of parallel spins along one of the in-plane axes and antiparallel along with the other (striped AFM configuration) [58, 59]. Also, the electronic structure proposes that AFM ordering produces the pairing interactions for the superconductivity in the FeSCs [59, 60]. With this background, in our samples upon increasing the calcium impurities and the decrement of T_{SDW}, it can be described that the Fe ions arrange striped AFM at the lower temperatures and so T_C declines. Moreover, Fig. 7a presents a similar trend of decreasing for the T_{SDW} and T_C. As an important result, the spin-fluctuations have a direct and effective impact on the superconductivity mechanism of our samples. Likewise, as we described before based on the AG theory, the calcium ions act as scattering centers and hence, at the lower temperatures, the Fe ions arrange striped AFM. This means that nonmagnetic impurities can affect and suppress the T_{SDW} and correspondingly the T_C. Based on the five-orbital model, *S*. Onari et al. [33] theoretically had considered the effect of the local and low amount of impurity in FeSCs. They found that the fully gapped sign-reversing $S_{\pm}$ state, which is attributed to the spin-fluctuations theory, is very fragile against impurities, while the S_{++} state due to the orbital-fluctuation is constant for all amounts of impurity and has no effect on the superconductivity suppression (for more detail, see Fig. 8b). So the matching of our experimental phase diagram and the results of the above theoretical model confirm

Table 3 The T_C, T_{SDW} and T_S for our synthesized samples

Sample	T_C (K)	T_{SDW} (K)	T_S (K)
Nd-1111	53	–	–
Nd–Ca0.01	48	115	125
Nd–Ca0.025	27	43	145
Nd–Ca0.05	–	27	180

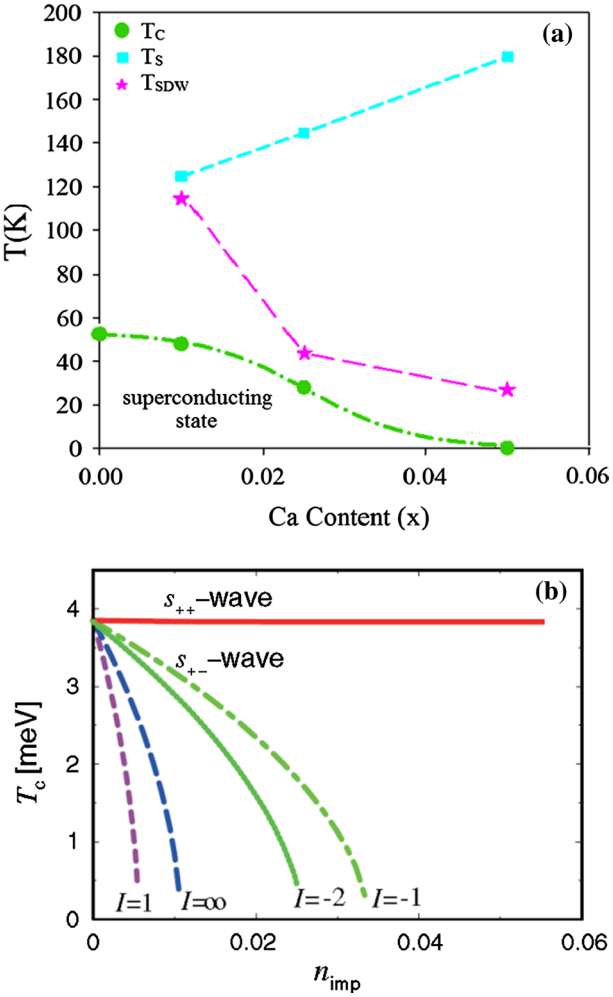

Fig. 8 **a** Phase diagram of our synthesized samples, **b** theoretical phase diagram for arbitrary nonmagnetic impurity taken from Ref. [33]

the role of the spin-fluctuations as a dominant pairing mechanism in our synthesized samples. In other words, the low amount of calcium impurity ($x \leq 0.05$) in our samples suppresses completely the superconductivity. Consequently and according to the mentioned theory, the $S_{\pm}$ symmetry and the spin-fluctuations are predominant against the orbital-fluctuations in our samples. In the other work, *J*. Li et al. [61] described that the T_C would be weakly suppressed by impurities in the S_{++} state, because of the following reasons: (1) suppression of the orbital-fluctuations because of the violation of the orbital degeneracy near the impurities and (2) the strong localization effect, in which the mean free path is comparable to the lattice spacing. Also, the angle-resolved photoemission spectroscopy (ARPES) confirms that when

the $S_{\pm}$ symmetry is dominant in comparison with the S_{++} state, identical impurity can suppress the superconductivity and the SDW states, simultaneously [62–64]. This behavior has occurred in our samples. Since the $S_{\pm}$ state that is attributed to the spin-fluctuations mechanism causes the superconductivity suppression for low amounts of calcium impurity in the synthesized samples, it can be concluded that the superconducting mechanism of our samples is the spin-fluctuations coupling.

4 Conclusions

To summarize, we have studied the superconducting behavior of the Nd-1111 iron-based superconductor that was doped by the calcium impurity. The samples were synthesized through the one-step solid-state reaction method. We found that:

1. Superconductivity is suppressed for the low amount of calcium impurity.
2. The T_C decreased linearly with the increase in impurity and also T_C reduced by increasing the residual resistivity. So, the calcium impurity acted as scattering centers and the Abrikosov–Gorkov theory is true for our samples.
3. In the phase diagram of our synthesized samples, upon increasing the calcium impurity, the temperature of the spin-density wave (T_{SDW}) state declined, so at the lower temperatures, the Fe ions arranged striped AFM.
4. According to the previous results and the matching of our experimental and the theoretical phase diagrams that can be concluded from the available theoretical model, the role of the spin-fluctuations (the $S_{\pm}$ state) has been confirmed as a dominant pairing mechanism in our samples.

Acknowledgements The authors are grateful to Vice Chancellor Research and Technology of Alzahra University for financial supports.

References

1. Y. Kamihara, M. Hirano, R. Kawamura, H. Yanagi, T. Kamiya, H. Hosono, J. Am. Chem. Soc. **128**, 10012 (2006)
2. N.L. Wang, H. Hosono, P. Dai, *Iron Based Superconductor: Materials, Properties and Mechanisms*, 1st edn. (CRC Press, Boca Raton, 2012), pp. 1–20
3. N. Fujiwara, S. Tsutsumi, S. Iimura, S. Matsuishi, H. Hossono, Y. Yamakawa, H. Kontani, Phys. Rev. Lett. **111**, 097002 (2013)
4. K. Gofryk, B. Saparov, T. Durakiewicz, A. Chikina, S. Danzenbacher, D.V. Vyalikh, M.J. Graf, A.S. Sefat, Phys. Rev. Lett. **112**, 186401 (2014)
5. H. Hosono, K. Kuroki, Physica C **514**, 399 (2015)
6. M. Calamiotou, D. Lampakis, N.D. Zhigadlo, S. Katrych, J. Karpinski, A. Fitch, P. Tsiaklagkanos, E. Liarokapis, Physica C **527**, 55 (2016)
7. V. Stanev, J. Kang, Z. Tesanovic, Phys. Rev. B **78**, 184509 (2008)
8. A.V. Chubukov, M. Khodas, R.M. Fernandes, Phys. Rev. X **6**, 041045 (2016)
9. P.C. Canifield, S.L. Bud'ko, Annu. Rev. Condens. Matter Phys. **1**, 27 (2010)
10. S. Matsuishi, T. Hanna, Y. Muraba, S.W. Kim, J.E. Kim, M. Takata, S. Shamoto, R.I. Smith, H. Hosono, Phys. Rev. B **85**, 014514 (2012)

11. K. Hayashi, P.V. Sushko, Y. Hashimoto, A.L. Shluger, H. Hosono, Nat. Commun. **5**, 3515 (2014)
12. H. Hosono, S. Matsuishi, Current Opinion Sol. State Mat. Sci. **17**, 49 (2013)
13. C. Fang, H. Yao, W.F. Tsai, J.P. Hu, S.A. Kivelson, Phys. Rev. B **77**, 224509 (2008)
14. T. Yildirim, Phys. Rev. Lett. **102**, 037003 (2009)
15. V. Chubukov, D.V. Efremov, I. Eremin, Phys. Rev. B **78**, 134512 (2008)
16. F. Kruger, S. Kumar, J. Zaanen, J. van den Brink, Phys. Rev. B **79**, 054504 (2009)
17. C. Chen, B. Moritz, J. van den Brink, T.P. Devereaux, R.R.P. Singh, Phys. Rev. B **80**, 180418 (2009)
18. W. Lv, J. Wu, P. Phillips, Phys. Rev. B **80**, 224506 (2009)
19. I. Eremin, J. Knolle, R.M. Fernandes, J. Schmalian, A.V. Chobokov, J. Phys. Soc. Jpn. **83**, 061015 (2014)
20. R.M. Fernandes, A.V. Chobokov, J. Schmalian, Nat. Phys. **10**, 97 (2014)
21. K. Kuroki, H. Usui, S. Onari, R. Arita, H. Aoki, Phys. Rev. B **79**, 224511 (2009)
22. K. Kuroki, Physica C **470**, S267 (2010)
23. W. Ly, F. Kruger, P. Phillips, Phys. Rev. B **82**, 045125 (2010)
24. T. Yamada, J. Ishizuka, Y. Ono, J. Phys. Soc. Jpn. **83**, 043704 (2014)
25. S. Onari, H. Kontani, Phys. Rev. Lett. **109**, 137001 (2012)
26. I.I. Mazin, D.J. Singh, M.D. Johannes, M.H. Du, Phys. Rev. Lett. **101**, 057003 (2008)
27. K. Kuroki, S. Onari, R. Arita, H. Usui, Y. Tanaka, H. Kontani, H. Aoki, Phys. Rev. Lett. **101**, 087004 (2008)
28. R.M. Fernandes, A.V. Chobukov, J. Knolle, I. Eremin, J. Schmalain, Phys. Rev. B **85**, 024534 (2012)
29. H. Kontani, T. Saito, S. Onari, Phys. Rev. B **84**, 024528 (2011)
30. H. Kontani, S. Onari, Phys. Rev. Lett. **104**, 157001 (2010)
31. Y. Yanagi, Y. Yamakawa, Y. Ono, Phys. Rev. B **81**, 054518 (2010)
32. Y. Yanagi, Y. Yamakawa, N. Adachi, Y. Ono, Phys. Rev. B **82**, 064518 (2011)
33. S. Onari, H. Kontani, Phys. Rev. Lett. **103**, 177001 (2009)
34. H. Kontani, Y. Inoue, T. Saito, Y. Yamakawa, S. Onari, Solid State Commun. **152**, 718 (2012)
35. T. Saito, S. Onari, Y. Yakamawa, H. Kontani, S.V. Borisenko, V.B. Zabolotnyy, Phys. Rev. B **90**, 035104 (2014)
36. D. Parker et al., Phys. Rev. B **78**, 134524 (2008)
37. Y. Bang, H. Choi, H. Won, Phys. Rev. B **79**, 054529 (2009)
38. T. Kariyado, M. Ogata, J. Phys. Soc. Jpn. **79**, 083704 (2010)
39. A.F. Wang, J.J. Pin, P. Cheng, G.J. Ye, F. Chen, J.Q. Ma, X.F. Lu, B. Lei, X.G. Luo, X.H. Chen, Phys. Rev. B **88**, 094516 (2013)
40. P. Cheng, B. Shen, F. Han, H. Wen, EPL **104**, 37007 (2013)
41. M. Sato, Y. Kobayashi, S.C. Lee, H. Takahashi, E. Satomi, Y. Miura, J. Phys. Soc. Jpn. **79**, 014710 (2010)
42. J. Li, Y. Guo, S. Zhang, S. Yu, Y. Tsujimoto, H. Kontani, K. Yamaura, E. Takayama, Phys. Rev. B **84**, 020513(R) (2011)
43. P.F.S. Rosa, C. Adriano, T.M. Garietezi, M.M. Piva, K. Mydeen, T. Grant, Z. Fisk, M. Nicklas, Sci. Rep. **4**, 6252 (2014)
44. J. Ishida, S. Limura, S. Matsuishi, H. Hosono, Phys. Condens. Matter. **26**, 435702 (2014)
45. F. ShahbazTehrani, V. Daadmehr, J. Supercond. Nov. Magn **32**(6), 1497 (2019). https://doi.org/10.1007/s10948-019-05197-3
46. Z. Alborzi, V. Daadmehr, Physica C **549**, 116 (2018)
47. Z. Alborzi, V. Daadmehr, J. Supercond. Nov. Magn. (2019). https://doi.org/10.1007/s10948-019-05209-2
48. A.A. Abrikosov, L.P. Gorkov, Sov. Phys. JETP **12**, 1243 (1961)
49. A.A. Abrikosov, Sov. Phys. Uspekhi **12**, 168 (1969)
50. P. Fulde, Mod. Phys. Lett. B **24**, 2601 (2010)
51. S.K. Malik, C.V. Tomy, P. Bhargava, Phys. Rev. B **44**, 7042 (1991)
52. A. Tavana, PhD. Thesis, Sharif university, Iran (2010)
53. P.G. Pagliuso, C. Rettori, S.B. Oseroff, P.C.C. Canfield, E.M. Baggio, D. Sanchez, Phys. Rev. B **57**, 3668 (1998)
54. E.M. Bittel, C. Adriano, C. Giles, C. Rettori, Z. Fisk, P.G. Pagliuso, J. Phys.: Cond. Matt. **23**, 455701 (2011)
55. J. Zhao, Q. Huang, C. Cruz, S. Li, J.W. Lynn, Y. Chen, M.A. Green, G.F. Chen, G. Li, Z. Li, J.L. Luo, N.L. Wang, P. Dai, Nat. Mater. **7**, 2315 (2008)

56. R.H. Liu et al., Phys. Rev. Lett. **101**, 087001 (2008)
57. A.F. Kordyuk, Low Temp. Phys. **38**, 888 (2012)
58. Y. Chen, J.W. Lynn, J. Li, G. Li, G.F. Chen, J.L. Luo, N.L. Wang, P. Dai, C. Dela Cruz, H.A. Mook, Phys. Rev. B **78**, 064515 (2008)
59. J. Paglione, R.L. Greene, Nat. Phys. **6**, 645 (2010)
60. I.I. Mazin, J. Schmalian, Physica C **469**, 614 (2009)
61. J. Li, Y.F. Guo, S.B. Zhang, J. Yuan, Y. Tsujimo, X. Wang, C.I. Sathish, Y. Sun, S. Yu, W. Yi, K. Yamaura, E. Takayama, Y. Shirako, M. Akaogi, H. Kontani, Phys. Rev. B **85**, 214509 (2012)
62. R.M. Fernandes, M.G. Vavilov, A.V. Chubukov, Phys. Rev. B **85**, 140512 (2012)
63. M.G. Vavilov, A.V. Chubukov, Phys. Rev. B **84**, 214521 (2011)
64. Y. Senga, H. Kontani, J. Phys. Soc. Jpn. **77**, 113710 (2008)

Publisher's Note Springer Nature remains neutral with regard to jurisdictional claims in published maps and institutional affiliations.